Wei, X., Zhou, Q., Li, F., Zhang, C., Sun, F., Zhang, Z., Li, R., Yu, H., Yan, Y., Li, L., Liermann, H., Speziale, S., Li, X. (2023): Novel High-Pressure Potassium Chloride Monohydrate and Its Implications for Water-Rich Planetary Bodies. - Journal of Geophysical Research: Planets, 128, 10, e2022JE007622.

https://doi.org/10.1029/2022JE007622

JGR Planets

RESEARCH ARTICLE
10.1029/2022JE007622

Novel High-Pressure Potassium Chloride Monohydrate and Its Implications for Water-Rich Planetary Bodies

Xinmiao Wei[1], Qiang Zhou[1], Fangfei Li[1], Caizi Zhang[1], Fuxing Sun[2], Zihan Zhang[1], Ruiyu Li[1], Hongyu Yu[1], Yalan Yan[3], Liang Li[1], Hanns-Peter Liermann[4], Sergio Speziale[5], and Xinyang Li[1,4,5]

[1]Synergetic Extreme Condition High-Pressure Science Center, State Key Laboratory of Superhard Materials, College of Physics, Jilin University, Changchun, China, [2]State Key Laboratory of Inorganic Synthesis and Preparative Chemistry, Jilin University, Changchun, China, [3]Institute for Interdisciplinary Biomass Functional Materials Studies, Jilin Engineering Normal University, Changchun, China, [4]Deutsches Elektronen-Synchrotron DESY, Hamburg, Germany, [5]GFZ German Research Centre for Geosciences, Potsdam, Germany

Abstract Saline water is a common fluid on the Earth's surface and in ice planets. Potassium chloride (KCl) is a common salt and is expected to be a ubiquitous solute in salt water in the Universe; however, few studies investigated the behavior of KCl-H_2O system at high pressures and temperatures. In this study, powder and single-crystal X-ray diffraction (SC-XRD), Raman and Brillouin scattering combined with diamond anvil cells were used to investigate the phase relation in the KCl-H_2O system for different KCl concentrations at 0–4 GPa and 298–405 K. The results of powder X-ray diffraction and Raman scattering demonstrate that a novel KCl hydrate is formed when KCl aqueous solutions transform to solid ice-VI and ice-VII at high pressure. Simultaneously, the single-crystal of KCl hydrate is synthesized from a supersaturated KCl solution at 298 K and 1.8 GPa. The structure is solved by SC-XRD, indicating a KCl monohydrate with the $P2_1/n$ space group is formed. We have verified the phase stability of KCl monohydrate by using Raman spectroscopy and density functional theory. Our results indicate that KCl monohydrate is a stable phase under pressure and temperature conditions between 1.6 and 2.4 GPa and 298–359 K. By considering the thermal profile and composition of icy moons, we hypothesize that the formation and decomposition of KCl monohydrate might induce mantle convection in these moons.

Plain Language Summary More and more evidence indicates that salt ions (Na^+, Ca^{2+}, Mg^{2+}, K^+, Cl^-, and SO_4^{2-}, etc.) could be dissolved in water and ices of the Earth-like planets and water-rich planets. The dissolution of alkali- and alkaline earth chlorides and sulfates in water and the incorporation of salt ions in the solid phases of H_2O ices have a significant effect on their chemical and physical properties. Potassium chloride (KCl) is a ubiquitous salt in the Universe, and we investigated the phase relationship of the KCl-H_2O system for different KCl concentrations at pressures of 0–4 GPa and temperatures of 298–405 K. We were able to produce a single crystal of KCl monohydrate by adding KCl into a KCl-saturated solution and pressurizing the solution at 1.8 GPa and 298 K. Our findings reveal the existence of a novel KCl monohydrate phase with monoclinic structure, which remains stable within the pressure and temperature range of 1.6–2.4 GPa and 298–359 K. Considering the thermal profile and composition of icy moons, our results suggest that the stability of the KCl monohydrate phase at pressures of 1.6–2.4 GPa and temperatures of 298–359 K may drive mantle convection through its formation and decomposition.

Key Points:

- A novel KCl monohydrate is synthesized in KCl-H_2O system at high pressures
- Structure, phase stability, and density of KCl monohydrate are determined at high pressures and temperatures
- KCl monohydrate formation and decomposition potentially drive mantle convection in icy moons

Supporting Information:

Supporting Information may be found in the online version of this article.

Correspondence to:

X. Li and F. Li,
lixinyang@jlu.edu.cn;
lifangfei@jlu.edu.cn

Citation:

Wei, X., Zhou, Q., Li, F., Zhang, C., Sun, F., Zhang, Z., et al. (2023). Novel high-pressure potassium chloride monohydrate and its implications for water-rich planetary bodies. *Journal of Geophysical Research: Planets*, *128*, e2022JE007622. https://doi.org/10.1029/2022JE007622

Received 15 OCT 2022
Accepted 13 SEP 2023

Author Contributions:

Conceptualization: Xinyang Li
Data curation: Xinmiao Wei, Xinyang Li
Formal analysis: Xinmiao Wei, Caizi Zhang, Fuxing Sun, Zihan Zhang, Ruiyu Li, Hongyu Yu, Yalan Yan, Xinyang Li
Funding acquisition: Qiang Zhou, Fangfei Li, Liang Li, Xinyang Li
Investigation: Xinmiao Wei, Caizi Zhang, Fuxing Sun, Zihan Zhang, Ruiyu Li, Hongyu Yu, Yalan Yan, Hanns-Peter Liermann, Sergio Speziale, Xinyang Li
Methodology: Xinyang Li
Project Administration: Qiang Zhou, Fangfei Li, Liang Li, Xinyang Li
Resources: Qiang Zhou, Fangfei Li, Liang Li, Hanns-Peter Liermann, Sergio Speziale, Xinyang Li
Supervision: Fangfei Li, Xinyang Li
Validation: Xinyang Li
Writing – original draft: Xinmiao Wei

1. Introduction

Water is necessary for planets' habitability and the high-pressure phases of H_2O are key constituents of many planetary bodies (Fortes & Choukroun, 2010; Journaux et al., 2020; Lammer et al., 2009; Nimmo & Pappalardo, 2016; Noack et al., 2016; Schubert et al., 2010; Vance et al., 2021). Mars Advanced Radar for Subsurface and Ionosphere Sounding radar data reveal that hypersaline perchlorate brines exist in the south pole of Mars (Lauro et al., 2021) and discrete amounts of Na^+, Ca^{2+}, Mg^{2+}, K^+, Cl^-, and SO_4^{2-} ions dissolved in water exist in the subsurface ocean of Europa and Callisto (Khurana et al., 1998; Kivelson et al., 2000; Zimmer et al., 2000; Zolotov & Shock, 2001). The incorporation of such ions in high-pressure ice could have a substantial impact on the thermal structure and the internal dynamics of these ice planets (Journaux et al., 2013, 2017; Vance et al., 2014; Zolotov, 2012). The characteristics of a number of binary H_2O-solute systems have been investigated to understand the internal

Writing – review & editing: Hanns-Peter Liermann, Sergio Speziale, Xinyang Li

structure of these planetary bodies (Frank et al., 2006, 2016; Journaux et al., 2017; Schmidt & Manning, 2016; Valenti et al., 2012). Sodium chloride (NaCl) is the most abundant salt dissolved in Earth's oceans and is present in ice planetary bodies. Dissolved NaCl considerably broadens the liquid phase stability field at the expense of those of both ice-VI and ice-VII (Journaux et al., 2013). Moreover, one study indicates that Na^+ and Cl^- ions can be incorporated into the structure of ice-VII leading to a significant expansion of the lattice parameter (Ludl et al., 2017). High pressure experimental studies of lithium chloride (LiCl) aqueous solutions yield similar results as for NaCl (Bove et al., 2015; Klotz et al., 2009). Moreover, the incorporation of Li^+ and Cl^- ions in H_2O solids hinder the proton ordering and delay ice-VII to ice-X transformation to a higher pressure than the pure system; such effect could possibly be responsible for the observed anomalous magnetic moment of Uranus and Neptune (Bove et al., 2015).

Some studies uphold that the salt-water systems could form solid hydrates at the pressure and temperature conditions of the planetary hydrosphere (Nakamura & Ohtani, 2011; Tsironi et al., 2020; Uriarte et al., 2015). Magnesium heptahydrate, $MgSO_4 \cdot 7H_2O$ can be formed in the $MgSO_4$-H_2O system at 0–4 GPa and 298–500 K (Nakamura & Ohtani, 2011). Furthermore, high pressure studies on 15 and 25 mass% NaCl aqueous solutions have shown that hydrohalite ($NaCl \cdot 2H_2O$) and an unidentified columnar hydrate can be formed at 1.1–1.3 GPa (Valenti et al., 2012). Recently, there have been reports of three distinct NaCl hydrates forming under conditions of high pressure and low temperature. These hydrates include one needle-like crystalline hydrate with an unknown composition and two with known compositions: $2NaCl{\cdot}17H_2O$ (SC8.5) and $NaCl{\cdot}13H_2O$ (SC13) (Journaux et al., 2023). However, very little is known about the system KCl-H_2O at high pressures, even though KCl is one of the most common salts in icy planetary environments (Yoshimura et al., 2004). The recent study by Frank et al. (2016) demonstrates that 1.6 mol% KCl could be incorporated into the structure of ice-VII up to 32.89 GPa at 295 K, and that the incorporation of KCl lowers the melting temperature of ice-VII by 45–80 K between 4 and 11 GPa.

^{40}K is a potassium radioisotope with a long half-life, which plays an important role in the thermal evolution of the Earth and other planets. Therefore, the presence of radiogenic ^{40}Ar (a decay product of ^{40}K) in the Titan moon atmosphere implies that significant amounts of ^{40}K may leak from Titan's core (Castillo-Rogez & Lunine, 2010). In addition, the decay of ^{40}K was also believed to be an important heat source for the thermal evolution of Europa (Chyba & Hand, 2001). Based on geochemical modeling, Zolotov and Shock (2001) suggest that dissolved chlorides might be enriched in the ocean of moons such as Europa. This enrichment of chloride and potassium ions in the subsurface oceans of icy planets, and the interactions in the KCl-H_2O system might strongly affect the planetary properties of ice giants. In this study, phase relation in the system KCl-H_2O is investigated up to 4 GPa pressure and in the temperature at 298–405 K and a novel KCl monohydrate is discovered to coexist with high-pressure H_2O ice phases. In addition, a method is proposed to grow a single-crystal KCl monohydrate (Kh) by using a supersaturated KCl solution at high pressure and room temperature. The phase stability of Kh is confirmed by Raman spectra and density functional theory (DFT), indicating that the Kh is a stable phase between 1.6 and 2.4 GPa and 298–359 K. Our findings have key implications for the dynamic structure of ice giants and low-mass exoplanets.

2. Methods

2.1. Sample Preparation and High-Pressure Experiments

All of the aqueous solutions containing KCl in various concentrations were prepared at room temperature by dissolving KCl (Sinopharm Chemical Reagent Co., Ltd., ≥99.8%) in deionized water. The concentrations of KCl solutions were 0.9, 1.8, 2.6, 3.1, 3.5, and 5.1 mol%. The respective KCl aqueous solutions were directly injected into the diamond anvil cells (DACs) by using syringes, and DACs were quickly sealed to prevent evaporation loss of H_2O. For the experiment dedicated to the synthesis of single-crystal Kh, a $100 \times 80 \times 25$ μm^3 single-crystal KCl in was loaded into a DAC, then a drop of KCl saturated solutions was immediately injected into the DAC by using a syringe, and the DAC was quickly sealed. For Raman and Brillouin spectroscopy, BX-90 type DACs with a 90° opening angle were used in all the experiments. The sample chambers were produced by laser drilling pre-indented T301 stainless steel or rhenium gaskets. High pressure heating was achieved by powering a cylindrical alumina ceramic heater positioned inside the body of the externally heated BX-90-type DACs. The alumina heater was wound using Pt wires with a 200 μm diameter. The temperature was measured by means of a K-type thermocouple, which was placed ~500(10) μm

away from the piston diamond's culet. The size of the sample chambers was fixed to 130 in diameter and 45 μm thickness to keep the uniformity between the experiments performed on solutions with different KCl concentrations. For powder X-ray diffraction (XRD) experiments, we used normal symmetric DACs equipped with 300 μm diamond culets. Rhenium gaskets were indented to 30 μm thickness and cylindrical sample chambers were produced by drilling 200 μm diameter holes using a laser drilling machine. Boehler-Almax design diamonds (400 μm culet size) were used at both sides in the DAC in the single-crystal X-ray diffraction (SC-XRD). In these experiments, the initial thickness of the gasket was 30 μm, and the sample chamber was 200 μm in diameter.

2.2. Raman Spectroscopy

High pressure and high pressure-temperature (high P-T) Raman spectra were collected using a LabRAM HR spectrometer (Horiba Jobin Yvon, France) with a 600 gr/mm grating. A solid-state single longitudinal mode laser (MSL-FN-532, Changchun New Industries Optoelectronics Technology Co., Ltd, China) was used as the excitation source to irradiate the samples inside the DACs. To avoid heating of the samples, the laser power was kept at 2 mW and the acquisition time was 60 s at each pressure point. The samples were compressed with the step of ∼0.1 GPa to approximately 4 GPa. The pressure was calibrated using a ruby sphere (Shen et al., 2020) and a small chip of Sm:SrB_4O_7 (Romanenko et al., 2018) for high pressure and high P-T experiments, respectively. The high P-T experiments were conducted along isothermal compression paths, the difference between the individual isotherms was 15 K. Temperature stability along the isotherms was maintained by a feedback power control unit; the uncertainty on temperature was below ±5 K.

2.3. Powder XRD

The 0.9, 1.8, 2.6, 3.1, 3.5, and 5.1 mol% aqueous KCl solutions were used to conduct the XRD experiment at 0–4 GPa at 298 K. High pressure XRD patterns were collected at the Extreme Conditions Beamline (ECB, P02.2) of the PETRA III synchrotron light source, DESY (Liermann et al., 2015). The energy of the beam was tuned to 42.7 keV, while the beam was focused to 3×8 μm^2 (horizontal × vertical, full width at half maximum). Samples to detector distance and tilt of the detector were determined from XRD of a CeO_2 standard from NIST (674b) analyzed with the Dioptas software (Prescher & Prakapenka, 2015). The load was applied to the DACs by a gas-membrane system, and the stabilization time for each pressure point was about 5 min. Sample's pressure was determined from the unit-cell parameter of gold powder (purity > 99.95%) by using the Pressure-Volume EOS of Au (Fei et al., 2007).

2.4. SC-XRD

After the synthesis of single-crystal Kh, the SC-XRD was collected at the same beamline (ECB, P02.2, PETRA III, DESY). Data were collected in 0.5° steps across a ±30° rotation around a vertical axis. The single-crystal data were calibrated with a standard single-crystal of enstatite ($(Mg_{1.93}Fe_{0.06})(Si_{1.93}Al_{0.06})O_6$, *Pbca*, $a = 18.2391(3)$ Å, $b = 8.8117(2)$ Å, and $c = 5.1832(1)$ Å). The pressure was calibrated using ruby spheres (Shen et al., 2020). Crystal structures were solved using OLEX2 with a SHELXT backend (Dolomanov et al., 2009; Sheldrick, 2015). The structural models displayed were drawn using the software VESTA and ORTEP (Farrugia, 2012; Momma & Izumi, 2011).

2.5. Brillouin Scattering Spectroscopy

Brillouin spectroscopy measurements were performed at State Key Laboratory of Superhard Materials, Jilin University, China. Brillouin spectroscopy measurements are conducted on a Brillouin scattering system with a 3 + 3 pass tandem Fabry–Pérot interferometer (Sandercock, 1980). The symmetric forward scattering geometry is used in the experiments (Whitfield et al., 1976). The exciting source is the 532 nm green laser with an output power of 100 mW. The acoustic velocities of liquid are calculated from the measured Brillouin frequency shifts as:

$$\upsilon = \Delta\nu_B \lambda_0 / \left[2 \sin \frac{\theta}{2}\right], \quad (1)$$

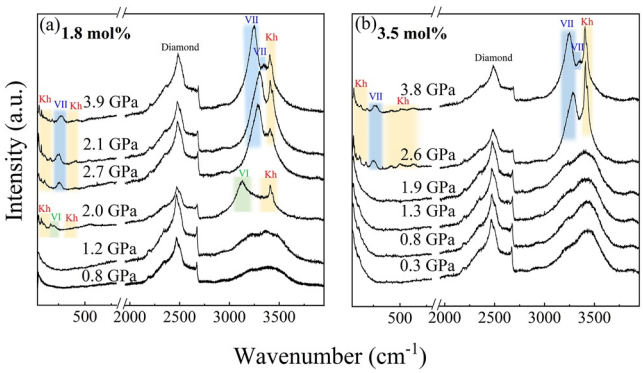

Figure 1. *Representative high-pressure Raman spectra of KCl solutions at* 298 K. (a) 1.8 mol% KCl solutions. (b) 3.5 mol% KCl solutions. The Raman modes of KCl monohydrate (Kh), ice-VI (VI), and ice-VII (VII) are indicated by yellow, green, and blue regions, respectively.

where υ is the acoustic velocity, $\Delta\nu_B$ is the measured Brillouin frequency shift, λ_0 is the laser wavelength of 532 nm, and θ is the external scattering angle of 60°. The pressure was calibrated using a ruby sphere (Shen et al., 2020).

2.6. Ab Initio Computations

Density functional theory (DFT) calculations were performed using the Vienna ab initio simulation package with generalized gradient approximation of the Perdewe-Burkee-Ernzerhof (PBE) exchange-correlation functional and projector augmented wave potentials (PAW) (Kresse & Furthmüller, 1996a, 1996b; Kresse & Joubert, 1999; Perdew & Wang, 1992; Perdew et al., 1996). The cutoff energy was set to 800 eV, criterion for energy convergence was 10^{-7} eV, and a 0.025 $Å^{-1}$ Monkhorst-Pack k-points grid was used for structural relaxations; the DFT-D3 method (Grimme et al., 2010) was used to account for the van der Waals interactions. The valence electrons of the pseudopotentials are $3s^23p^64s^1$ for K, $3s^23p^5$ for Cl, $2s^22p^4$ for O and $1s^1$ for H, respectively. Positions of K, Cl and O atoms in the crystal structure of Kh were from SC-XRD data, and the positions of H atoms were from ab initio structural relaxations as discussed in Results. The simulated XRD data of K, Cl, and O atoms in theoretically obtained crystal structure with H agrees with that from experiments.

3. Results

3.1. Results of Raman Scattering and XRD of KCl Solutions at High Pressures and Room Temperature

Representative Raman spectra of ice polymorphs in experiments with 1.8 and 3.5 mol% KCl are shown in Figure 1. 1.8 mol% KCl aqueous solutions are compressed from 0.8 to 3.9 GPa at 298 K (Figure 1a). The liquid phase is observed from 0.8 to 1.2 GPa (Figure 1a). At 2.0 GPa, new peaks appear at ~200, 3,411.2(1), and 3,433.4(4) cm^{-1} in addition to the peaks of ice-VI at 176.2(3) and 3,125.5(5) cm^{-1} (Figure 1a). Ice-VI transforms to ice-VII at 2.7 GPa with a 0.6 GPa drop of the transition pressure and the peaks observed at 2.0 GPa are preserved across the transition and coexist with ice-VII up to 3.9 GPa (Figure 1a). In the experiment performed on 3.5 mol% KCl solutions, the ice-VI phase is not detected at high pressures (Figure 1b). Several new Raman vibration modes at ~200, 3,410.2(8), and 3,424.7(1) cm^{-1} are also observed at pressures above 2.6 GPa.

Figure 2 illustrates representative high pressure XRD patterns of 2.6 mol% KCl aqueous solutions at high pressures and room temperature. The broad diffraction feature at 2θ ~6° indicates that the sample is a liquid phase at 1.8 GPa. Upon further compression, numerous sharp Bragg peaks emerge at 2.3 GPa in addition to the reflections of gold, which indicate the formation of solid phases from the initial solution. In addition to the reflections of ice-VI, several other new peaks are also observed in the XRD pattern (Figure 2a). With further compression, the pressure drops to 2.1 GPa at the transition from ice-VI to ice-VII, and the additional reflections first observed at 2.3 GPa are still present. After comparing with KCl-B1 and KCl-B2 phases, we find that these new peaks cannot be indexed by the known KCl phases. Previous studies indicated that KCl could be incorporated into the structure of ice-VII, which would not produce any new diffraction peaks other than the peaks of ice-VII (Frank et al., 2016). Based on our single-crystal analysis (details can be found in next section), the new peaks could be assigned to a newly discovered Kh with a space group of $P2_1/n$ (Figure 2b). Based on XRD and Raman scattering results at 298 K, the concentration-pressure cross-section of the KCl-H_2O phase relation is determined up to 4 GPa (Figure 3). However, the precise phase boundary between liquid and ice (ice-VI/VII) was not defined in this experiment because the majority of the experimental samples were supercooled solutions and the liquid may have been present as a metastable phase. We thus only show the experimental results in Figure 3.

3.2. Synthesis, Structure, and Thermal Stability of Kh at High Pressure

Given the fact that all the peaks of Kh are mixed with ices (ice-VI and ice-VII), it is difficult to analyze the structure of Kh. To determine the structure of Kh, a method is proposed to synthesize the pure Kh at high

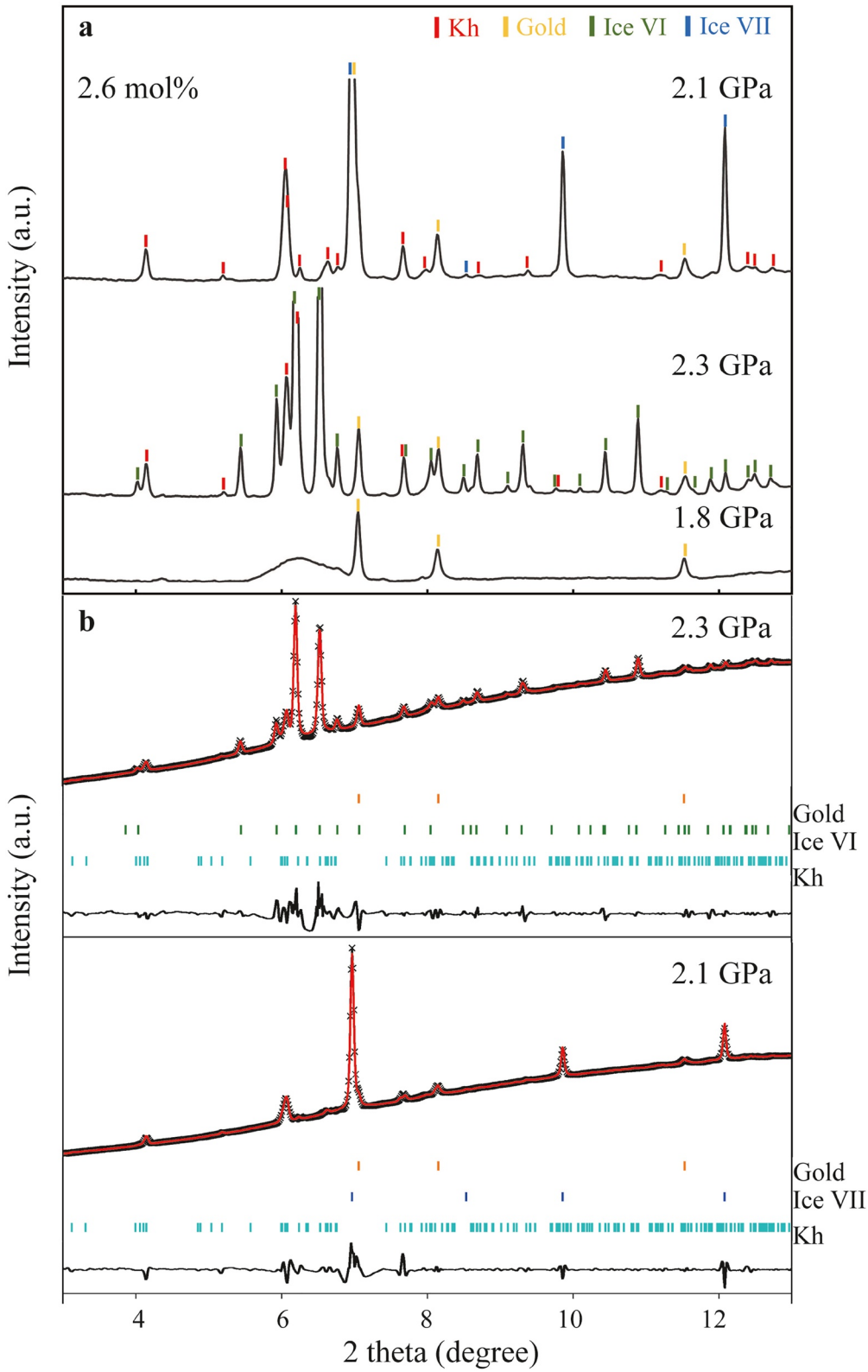

Figure 2. *X-ray diffraction patterns of* 2.6 mol% KCl *solutions at high pressures and* 298 K. The sequence of patterns represents the temporal evolution along the compression experiment from 1.8 to 2.3–2.1 GPa after pressure dropped at the Ice-VI to ice-VII transition. (a) Colored tick marks show the diffraction peak positions of Gold (yellow lines), ice-VI (green lines), ice-VII (blue lines), and Kh (KCl monohydrate, red lines). (b) Lebail refinement of 2.6 mol% KCl in H_2O at 2.3 GPa ($wR = 0.52\%$) and 2.1 GPa ($wR = 0.41\%$), respectively. Red line: refined results; black cross: collected data. The X-ray wavelength is 0.2885 Å.

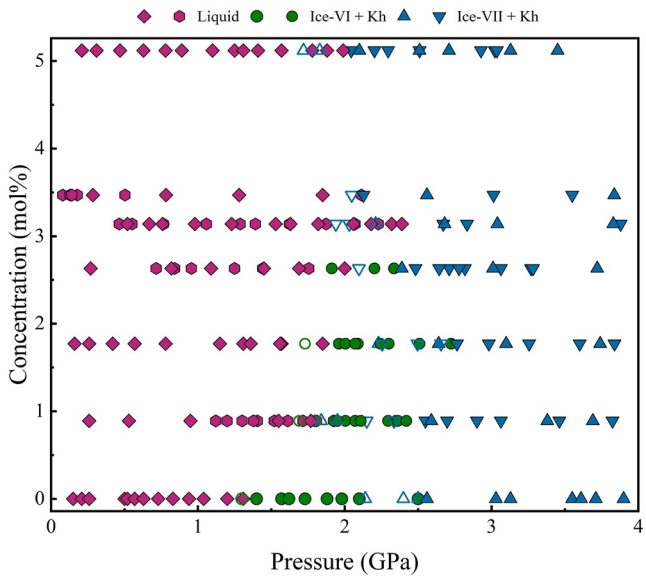

Figure 3. *Phase relation of* KCl-H_2O *system at* 298 K. The purple diamonds (liquid), green solid circles (ice-VI + Kh) and blue regular solid triangles (ice-VII + Kh) correspond to the data of Raman scattering. The open green circles and open blue triangles represent ice-VI and ice-VII observed after the pressure drop due to phase transitions. The hexagons (liquid), green solid circles with a point (ice-VI + Kh) and blue inverted solid triangles (ice-VII + Kh) correspond to the data from X-ray diffraction. The open green circles with a point and the open blue inverted triangles represent ice-VI and ice-VII observed after the pressure drop caused the phase transitions.

pressure (see Section 2.1). The pressure is increased to 1.8 GPa at 298 K by a gas-membrane system and a columnar hydrate with 20 × 117 μm^2 size grows from the liquid after 10 min stabilization (Figure 4). The Raman spectra and XRD indicate that the Kh is pure without any contamination of ices (Figures 4 and 5). In addition, new peaks occur at ∼3,414(1), ∼3,432(6), ∼200, and ∼600 cm^{-1} are consistent with Kh (Figure 4). The main peaks in SC-XRD are also consistent with powder XRD. The visible peaks of powder XRD is less than SC-XRD, which should be due to limited KCl content in unsaturated KCl solutions. On the basis of the pure SC-XRD data, the structure of Kh can be well determined.

SC-XRD indicates that the KCl hydrate is a monohydrate at 1.8 GPa and 298 K and unit cell parameters of the Kh are a = 5.7058(8) Å, b = 6.3889(12) Å, c = 8.4556(15) Å and β = 107.34(2)°. The information for the structural refinements based on SC-XRD measurements is shown in Table 1 and a figure of the structure showing the 50% ellipsoids is shown in Figure S1 in Supporting Information S1. This phase is distinct from the crystal lattices of the B1 or B2 phases of KCl under these conditions. In contrast to $MgCl_2 \cdot 8H_2O$, $MgCl_2 \cdot 12H_2O$, and $MgBr_2 \cdot 6H_2O$ (Hennings et al., 2013), the KCl hydrate has a lower water number. The K atom is bonded to 3 water molecules and 5 Cl atoms in the structure. In addition, each Cl is bonded to 5 K atoms (Figure 6). Similar to the $NaCl_2 \cdot H_2O$ structure (Bode et al., 2015), each O atom in the Kh structure is shared by two K atoms. The position of hydrogen is difficult to be determined by SC-XRD due to its weak scattering signal. To overcome this challenge, we employed ab initio calculations in the K-Cl-O sublattice to determine the hydrogen positions, which were then validated by SC-XRD. Water molecules in Kh exhibit strong polarity in their H-O bonds, with H atoms typically oriented toward negative charges in Kh. Given the negative charge of Cl^- ions and the fact that O^{2-} ions have two nearest neighbor Cl^- ions in this sublattice of K, Cl, and O, we positioned the H atoms between the nearest Cl and O atoms. We then performed ab initio structural relaxation to obtain the final structures. The results from this investigation agreed with both the XRD patterns for the crystal structure from structural relaxation and the experimental SC-XRD data. The crystal structures from both SC-XRD and ab initio structural relaxation can be found in Supporting Information S1.

To test the stability of Kh, we conducted high P-T Raman experiments along six different P-T paths covering a range of pressures and temperatures (1.6–3.0 GPa and 298–405 K), as shown in Figures 7 and 8. We synthesized Kh at room temperature and then compressed and heated it to high pressure and temperature. For instance, we synthesized three single-crystals of Kh at 2.1 GPa and 298 K in DAC (Figure 7a), gradually increased the temperature by 5–15 K interval, and collected Raman spectra to determine the phases in the sample chamber. Our findings reveal that Kh remains stable up to 2.1 GPa and 333 K. However, the pressure abruptly dropped to 1.5 GPa when the temperature was increased to 346 K, and the Raman modes of Kh vanished; we suspect that the crystals were in the KCl-B1 phase at 1.5 GPa (Figure 7b). We then increased pressure up to 1.9 GPa at 346 K, at which Kh recrystallized. We subsequently raised the temperature to 405 K at this pressure and found that the system transformed into a liquid and solid phase, with the Raman spectra indicating the decomposition of Kh. As the solid and liquid were cooled from 405 to 359 K at 2.0 GPa, both the Raman spectra and sample image showed the formation of Kh (Figure 7). However, the observed Kh at temperatures higher than 360 K is believed to be a metastable phase, given that the temperature is about 20 K lower than that of the heating experiment. By using the above method, we tested the thermal stability of Kh over a range of pressures and temperatures (0–4 GPa and 298–405 K), and the results are presented in Figure 8. Since the melting temperature of Kh is approximately 10 K higher than that of pure ice VI (Bezacier et al., 2014) and 30 K higher than 1.6 mol% KCl ice-VII (Frank et al., 2016) at ∼2 GPa, respectively, we conclude that Kh is a thermally stable phase, as proposed in a previous study (Journaux et al., 2023).

Isothermal compression experiments reveal that Kh decomposes to ice-VII at 2.7 at 318 and at 2.4 GPa at 336 K. Interestingly, the pressure of decomposition is consistent with the phase boundary between KCl-B1 and KCl-B2

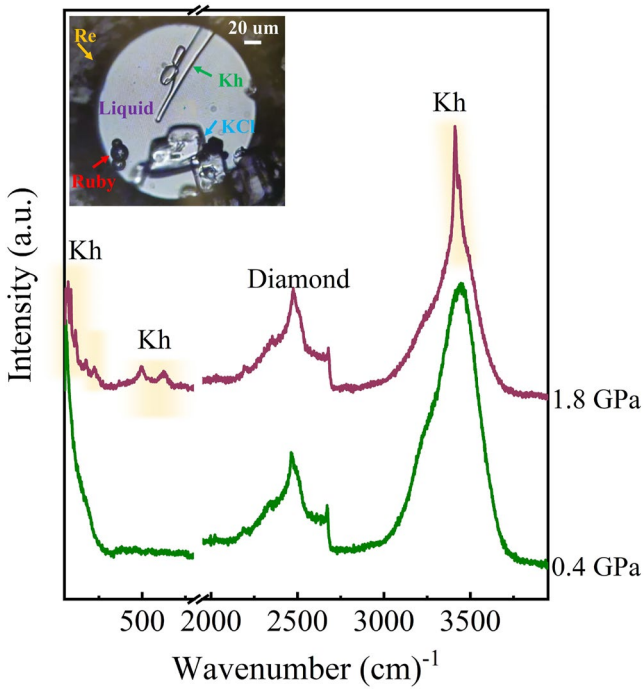

Figure 4. *The Raman spectra of single-crystal* KCl *monohydrate*. The Raman spectra of the supersaturated KCl-water system at 0.4 and 1.8 GPa indicating the liquid phase and KCl monohydrate (Kh), which are represented by green (liquid) and purple (Kh) lines, respectively. The inset shows the sample chamber. Re, Ruby, and Kh represent Re gasket, ruby spheres, and KCl monohydrate, respectively. The transparent section of the sample chamber represents the liquid.

phases (Walker et al., 2002). To further investigate the stability of Kh, DFT calculations were performed at pressures ranging from 2 to 10 GPa for various phases, including Kh, ice-VI + KCl-B1, ice-VII + KCl-B1, ice-VI + KCl-B2, and ice-VII + KCl-B2. As depicted in Figure S2 in Supporting Information S1, the $P2_1/n$ phase of Kh has a lower enthalpy than ice-VI + KCl-B1 or ice-VII + KCl-B1 when the pressure exceeds 3 GPa, indicating that Kh is thermodynamically stable against dissociation into KCl-B1 + salty aqueous solution. However, when dissociation into KCl-B2 + salty aqueous solution was considered, Kh was found to be thermodynamically metastable. This is because the KCl sublattice of Kh is nearly isomorphic to KCl-B1, and high pressures favor the transformation to KCl-B2. Consequently, the stable region of Kh is consistent with that of KCl-B1. It should be noted that the DFT calculations were conducted at 0 K, and therefore, the computed pressure at which Kh is thermodynamically stable (~3 GPa) is 1 GPa higher than observed (~2 GPa) in the experiments performed at ambient and high temperatures.

3.3. Brillouin Scattering Spectroscopy at 298 K

The acoustic velocities (v) of 1.8 and 5.1 mol% KCl solutions were measured up to 1.8 GPa at 298 K (Table 2, Figure S3 in Supporting Information S1). The acoustic velocities are related to the isentropic change of density (ρ) with pressure by Kell and Whalley (1975):

$$\left(\frac{\partial \rho}{\partial P}\right)_S = \frac{1}{v^2}, \tag{2}$$

where S is the entropy. Hence, from the isentropic process to the isothermal process, there are related corrections:

$$\left(\frac{\partial \rho}{\partial P}\right)_T = \frac{1}{v^2} + \frac{T \cdot \alpha_P^2}{C_P}, \tag{3a}$$

$$\alpha_P = -\frac{1}{\rho} \cdot \left(\frac{\partial \rho}{\partial T}\right)_P, \tag{3b}$$

$$\left(\frac{\partial C_P}{\partial P}\right)_T = -T \cdot \left(\frac{\partial^2 v_{sp}}{\partial T^2}\right)_P = -\frac{T}{\rho} \cdot \left[\alpha_P^2 + \left(\frac{\partial \alpha_P}{\partial T}\right)_P\right]. \tag{3c}$$

Where P is the pressure, T is the temperature, α_P is the coefficient of thermal expansion, C_P is the specific heat capacity, and ν_{sp} is the specific volume. The density of KCl solutions was calculated from the measured v by recursive integration of Equations 3a–3c (Abramson & Brown, 2004; Mantegazzi et al., 2013; Wiryana et al., 1998). The calculation starts with the integration of Equation 3a at 1 bar and the values of ρ and C_P are from literature data (Pabalan & Pitzer, 1988; Romankiw & Chou, 1983). The reference values of $\frac{\partial \alpha_P}{\partial T}$ in different KCl concentrations were obtained from Jones et al. (1948) and Apelblat and Manzurola (1999), respectively. The first iteration step is performed assuming that the isothermal-adiabatic correction term ($\frac{T \cdot \alpha_P^2}{C_P}$) is negligible. The resulting density is used to calculate a first approximation of α_P and C_P (Equations 3b and 3c) that are further used in the second iteration of Equation 3a without neglecting the isothermal-adiabatic correction term. This process was repeated until convergence was reached. As a result, the relation between pressure and density can be derived from Equation 3 (Table 2). The result indicates that the dissolution of 1.8 mol% KCl into water could increase the density of pure water (Li et al., 2005) by 1.4%–4.8% from 0.3 to 0.9 GPa (Figure 9), respectively. The density of a 5.1 mol% KCl solution was found to be 9.2%–11% higher than pure water (Li et al., 2005).

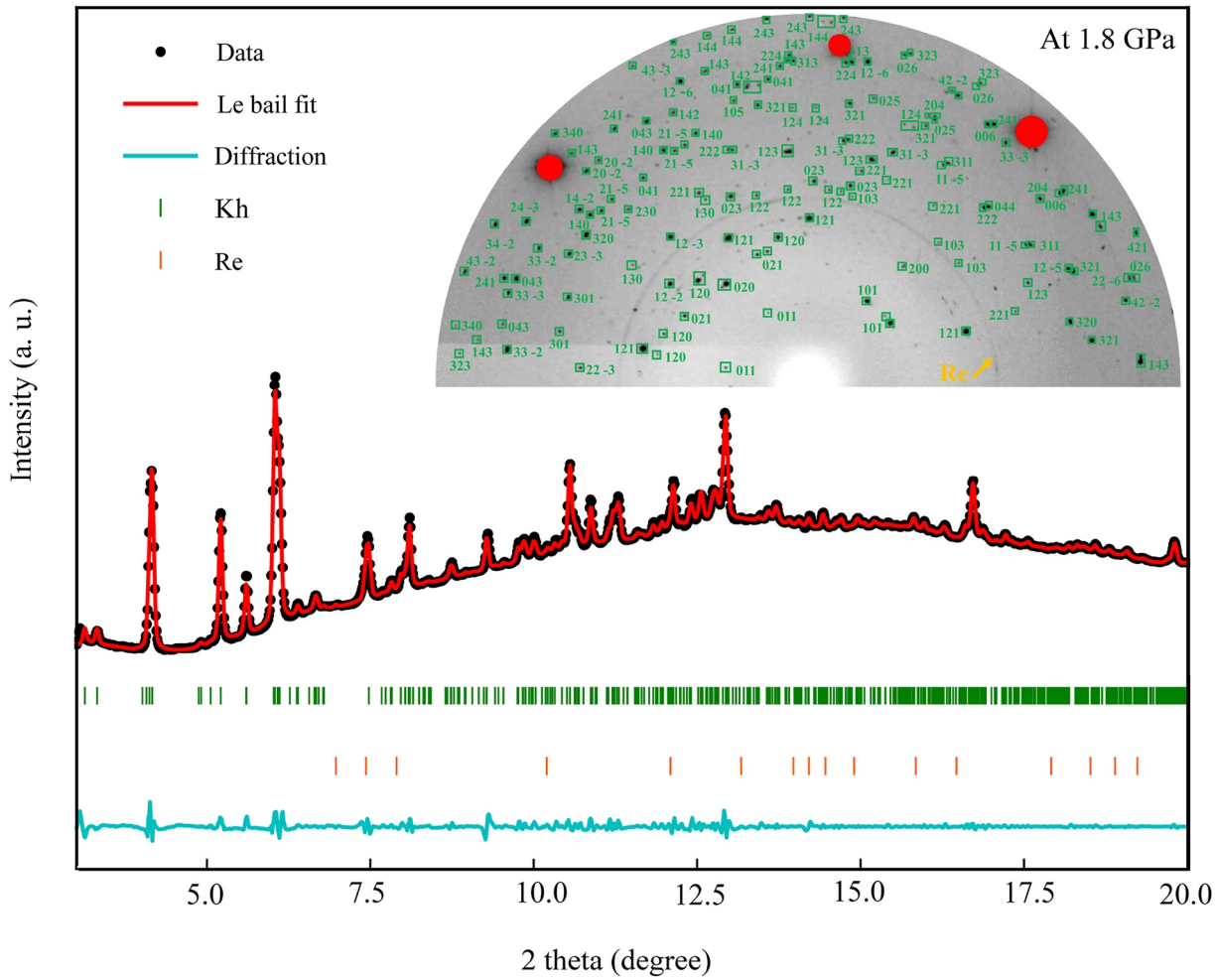

Figure 5. *Experimental X-ray diffraction image and the Le Bail refinement of the integrated pattern of single-crystal* KCl *monohydrate at* 1.8 GPa *and* 298 K. The experimental data, fit, and residues are shown in black, red, and blue, respectively. Kh (KCl monohydrate) and Re are indicated by green and orange sticks, respectively. The inset shows that the reflections of Kh and *hkls* are labeled. The diamond reflections are masked by red shadows.

4. Discussion

To date, there are still controversies on the solid phases assemblage in salt-water systems at high pressure. Two main mechanisms of salt incorporation exist in the high-pressure regimes. In the first one, salt ions are incorporated in the substitution of an H_2O molecule into the structure of ice-VII (Bove et al., 2015; Hernandez et al., 2022; Journaux et al., 2017; Klotz et al., 2009). In the second, salt ions form a new structure with H_2O, forming classical salt hydrates (Komatsu et al., 2015; Tsironi et al., 2020).

Some previous studies show that salts can be incorporated into the structure of ice-VII by incorporation of cation and anion species at interstitial sites at high pressures and different temperatures (Frank et al., 2006, 2016; Hernandez et al., 2022; Journaux et al., 2017; Klotz et al., 2009, 2016; Ludl et al., 2017). By the recrystallization of amorphous $LiCl \cdot 6D_2O$ under high pressure and low temperature, Klotz et al. (2009) indicate that Li^+ or Cl^- ions can be incorporated into the structure of ice-VII and result in the formation of "salty ice-VII." Using the same synthesis method as Klotz et al. (2009), another study indicates that 9.8 mol% NaCl can be incorporated into the structure of ice-VII between 2 and 4 GPa (Ludl et al., 2017). The H_2O-RbI system was studied by Journaux et al. (2017) using XRD and X-ray fluorescence up to 450 K and 4 GPa, and the results revealed that the incorporation of RbI enlarge unit cell volume of ice-VI and ice-VII by 1% in comparison to pure water ice. First-principles simulations predict that up to 2.5 wt.% NaCl is incorporated in dense water ice (ice-VII/X) in a way that both Na and Cl replace H_2O molecules (Hernandez et al., 2022). By compressing aqueous solutions of NaCl and KCl at room temperature, two studies claim that at least 2.4 NaCl and 1.6 mol% KCl can be incorporated into the

Table 1
Information for the Structural Refinements Based on Single-Crystal X-Ray Diffraction Measurements

Chemical composition	$KCl \cdot H_2O$
Pressure and temperature	1.8 GPa and 298 K
Cell setting, space group	Monoclinic, $P2_1/n$
a, b, c (Å)	5.7058(8), 6.3889(12), 8.4556(15)
β (°)	107.34 (2)
Volume (Å^3)	294.224
Specimen shape (μm)	20×117 μm^2
X-ray radiation	Synchrotron, P02.2, ECB, DESY
Wavelength (Å)	0.2903
Exposure (s)	2 s
Range of h, k, l	$-8 \le h \le 8$
	$-7 \le k \le 7$
	$-11 \le l \le 11$
$R(F^2)$, %	8.32
$wR(F^2)$, %	27.78
Number of reflections	618
Number of fitted parameters	29

structure of ice-VII (Frank et al., 2006, 2016). However, in our study, using aqueous solutions as staring material and directly compressing the system, both Raman and XRD results indicate the formation of a novel KCl hydrate phase during the crystallization of ice-VI and ice-VII.

Many salt hydrates including $LiCl \cdot H_2O$, $NaCl \cdot xH_2O$ (x = 2, 8.5, 13), $MgCl_2 \cdot xH_2O$ (x = 1, 2, 4, 6, 10) and $CaCl_2 \cdot 6H_2O$ have been identified at different temperature and pressure conditions (Hönnerscheid et al., 2003; Journaux et al., 2023; Klewe & Pedersen, 1974; Komatsu et al., 2015; Sugimoto et al., 2007). Interestingly, even though KCl is one of the most studied halides, KCl hydrates have never been reported at low temperatures or at high pressures (Frank et al., 2016; Yoshimura et al., 2004). Our XRD and Raman measurements indicate that a Kh indeed forms at high pressures, and its crystal structure contains one water molecule in the primitive unit cell. The two Raman modes we observe at 3,410–3,424 cm^{-1} correspond to the symmetric stretching ν_1 and asymmetric stretching ν_3 of the water molecule in Kh structure (Figure 1). Moreover, other types of salt hydrates, such as antarcticite ($CaCl_2 \cdot 6H_2O$) and hydrohalite, have Raman peaks between 3,240 and 3,540 cm^{-1}, which are related to the vibration of water molecules (Baumgartner & Bakker, 2009; Valenti et al., 2012). Thus, we could confirm that the KCl in water-rich system prefers crystallizing KCl hydrate rather than forming a KCl-bearing ice-VII at high pressure. Nevertheless, the potential incorporation of KCl in the structure of ice-VII at relatively low salt concentration levels cannot be excluded, and whether the addition of KCl will alter the ice VI-VII boundary as measured by Pistorius et al. (1968) is still an open question. Besides, the behavior of the system when different starting materials are used and different high-pressure synthesis approaches are applied needs to be thoroughly investigated in the future.

5. Implications

5.1. Implication for Water-Bearing Diamond Inclusions From the Earth's Interior

Saline solutions are the most common liquid phases in the shallow Earth and in ocean worlds' interior (Chivers et al., 2021; Huang et al., 2019; Khurana et al., 1998; Zolensky, 2005). Inclusions in deep diamonds from the Earth's mantle transition zone indicate that 0.1–16.8 mol% (K, Na)Cl coexist with ice-VII, revealing the presence of saline fluids in the deep Earth's interior (Tschauner et al., 2018). KCl was found in sub-micrometer-size fluid inclusions of fibrous diamond (Smith et al., 2011) and it demonstrates that KCl-rich fluids are important phases in the Earth's interior. However, no KCl hydrates were reported in the ice-VII bearing diamond inclusions (Tschauner et al., 2018) and other microinclusions containing KCl (Logvinova et al., 2019); one possible

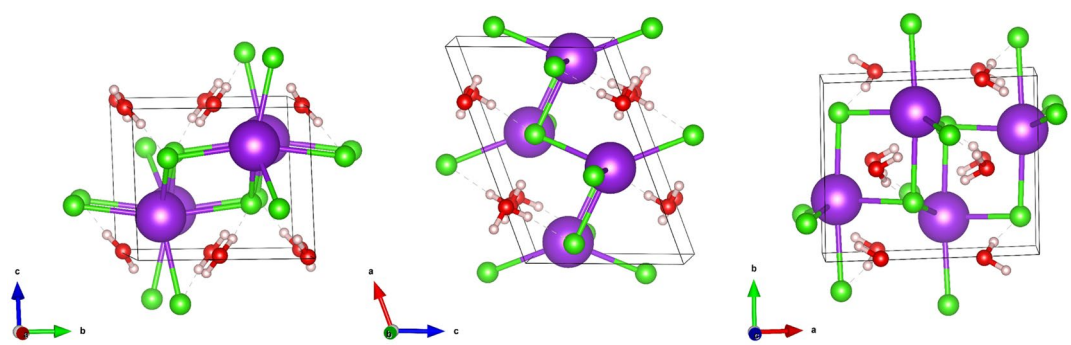

Figure 6. *Schematic representation of the crystal structure of* $KCl \cdot H_2O$ *in views approximately along a, b, and c-axis at* 1.8 GPa *and* 298K. The box with solid lines represents the unit cell. Different color spheres in the sites represent H (pink), K (purple), Cl (green), and O (red) atoms, respectively. The dotted line represents hydrogen bonds.

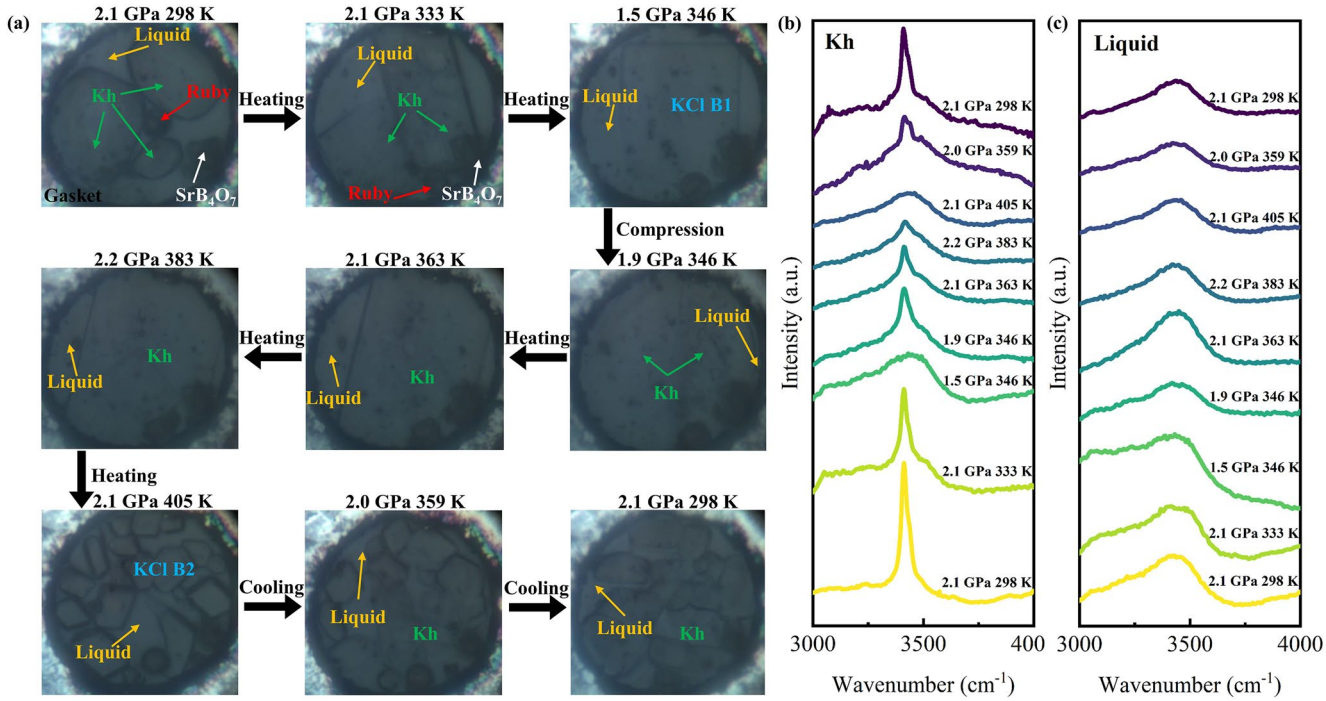

Figure 7. *Representative optical microscopy images of the sample and Raman spectra*. (a) Gasket, ruby, KCl-B1, KCl-B2, SrB_4O_7, and Kh represent Re gasket, ruby sphere, KCl-B1 phase, KCl-B2 phase, SrB_4O_7, and KCl monohydrate, respectively. The transparent section of the sample chamber represents the liquid. (b) The Raman spectra of Kh at various pressures and temperatures are represented with different colored lines. (c) The Raman spectra of liquid at various pressures and temperatures are plotted in different colors.

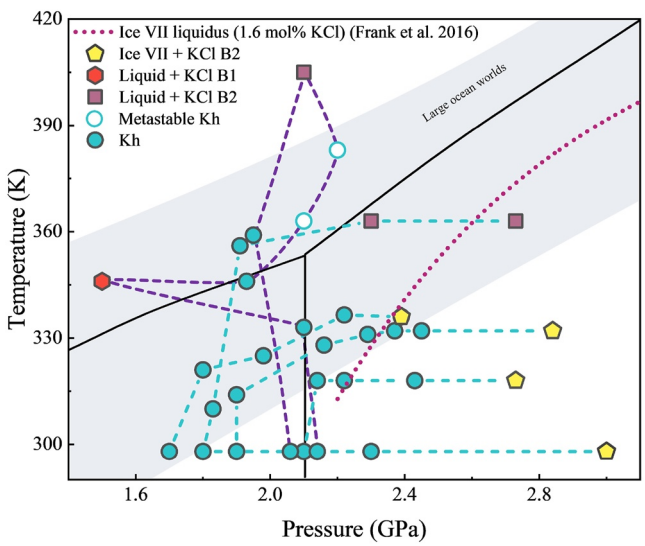

Figure 8. *Schematic phase diagram of the* KCl *monohydrate at high temperature and pressure*. The pure water phase diagram is shown as black lines (Journaux et al., 2013). The gray-shaded area depicts the approximate range of conditions present in ocean worlds (Journaux et al., 2020). The purple-dotted line represents the P-T path followed in our heating and quenching experiments.

explanation may be that in absence of any structural or spectroscopic information, the KCl hydrate phases were simply overlooked. Thus, the novel KCl monohydrate found in our study provides the basic structural information to characterize this phase in the water-salts-bearing diamond inclusions.

5.2. Implications for the Composition of Icy Moons

Subsurface conductivity in Jupiter's moon Europa inferred from remote magnetometry measurements by Galileo spacecraft indicates the presence of magnesium sulfate brine in subsurface ocean (Hand & Chyba, 2007). Based on geochemical modeling, Zolotov and Shock (2001) report that chloride salts might be abundant in Europa's ocean water. Furthermore, a study indicates that ice grains in Saturn's E-ring contain ~0.5–2 wt.% sodium salts, and could originate from an ocean below the surface of Enceladus (Postberg et al., 2009). Because of the fact that the radioactive decay of K produces ^{40}Ar, it was hypothesized that K may be leached from the hydrated silicate core and dissolved into the deep ocean, which leads to the enrichment of ^{40}Ar in Titan's atmosphere (Fortes, 2012; Niemann et al., 2005). Thus, K^+ and Cl^- can be present in the subsurface ocean of these icy moons and could play a crucial role in controlling the thermal properties of the subsurface ocean in ice giants.

Based on our results on the phase relations in the system KCl-H_2O, even if 0.9 mol% KCl is dissolved into the subsurface ocean and the Kh can be formed and coexist with ice (Figure 3). The measured densities of the H_2O-KCl fluids could help to understand the internal ocean structure of icy moons in the Solar System (Table 2, Figure 9). The dissolution of 1.8

Table 2
Measured υ and ρ of 1.8 and 5.1 mol% KCl Solutions at 298 K and High Pressures

1.8 mol%			5.1 mol%		
Pressure (GPa)	υ (km/s)	ρ (g/cm^3)	Pressure (GPa)	υ (km/s)	ρ (g/cm^3)
0.2(1)	2.02(4)	1.105(1)	0.3(1)	2.06(3)	1.203(1)
0.6(1)	2.23(4)	1.165(1)	0.6(1)	2.44(3)	1.222(1)
0.7(1)	2.66(3)	1.150(1)	0.8(1)	2.60(2)	1.236(1)
0.8(1)	2.88(3)	1.149(1)	0.9(1)	2.72(6)	1.240(1)
1.1(1)	2.97(4)	1.166(1)	1.0(1)	2.85(3)	1.241(1)
1.3(1)	3.16(4)	1.172(1)	1.2(1)	2.97(6)	1.259(1)
1.5(1)	3.09(9)	1.205(2)	1.5(1)	3.29(2)	1.259(1)
			1.6(1)	3.29(6)	1.267(1)
			1.8(1)	3.27(4)	1.294(1)

and 5.1 mol% KCl into water could increase the density ~7% and ~11% with respect to pure water at 1 GPa, respectively (Figure 9). There is also an upward shift of ~14% compared with pure water density at 1 GPa when adding 1.7 mol% NaCl (Mantegazzi et al., 2013). Besides, previous studies indicate that an aqueous $(NH_4)2SO_4$ ocean with 1.35 g/cm^3 density can be formed above an ice-VI shell in Titan's mantle (Fortes et al., 2007). Thus, the density for different KCl solutions provides essential data for planetary modeling.

Previous studies have proposed models of mantle convection induced by salty high-pressure ices in large icy moons and ocean exoplanets (Journaux, 2022; Journaux et al., 2017, 2023). Using the obtained densities and phase stability of KCl-H_2O compounds, we have shown that Kh may play a crucial role in the mantle dynamics of large ocean worlds (as illustrated in Figure 10). Kh could crystallize below the sub-surface ocean at depths corresponding to ~1.6 GPa. Due to its higher density compared to ice-VI/VII (as shown in Figure 9), the formed Kh would tend to move downward. Kh would decompose to the KCl-B2 phase and ice-VII at pressures higher than 2.4 GPa. In this case, KCl-B2 phase would continue to move downward because of its high density (as depicted in Figure 10) and finally reach the core mantle boundary and remain there in gravitational equilibrium due to its lower density than antigorite (taken as a proxy of the hydrated silicate rocky core). Moreover, if the ice melt is present at the core mantle boundary (Hernandez et al., 2022; Journaux, 2022), both the KCl-B2 phase and K^+ ions leached from the hydrated silicate core can dissolve into the melt. Given that

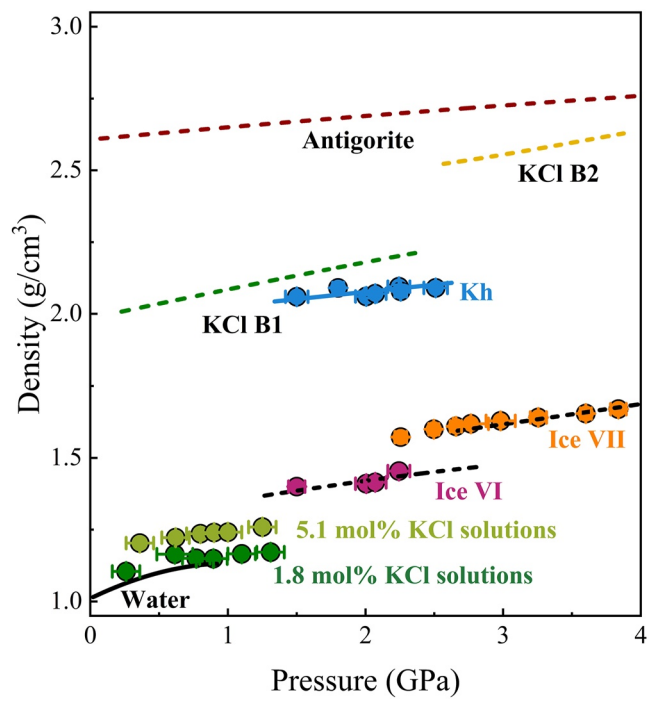

Figure 9. *Densities of possible components in ice giants at high pressure and* 298 K. Colored solid circles represent results in this study. Brown, orange, and blue circles represent the density of ice-VI, ice-VII, and Kh (KCl monohydrate), respectively. Green and light green circles represent the density of 1.8 and 5.1 mol% KCl aqueous solutions at high pressures and 298 K, respectively. The black solid line corresponds to the density of pure water determined by Li et al. (2005). The black dashed lines represent the density of pure ice-VI and ice-VII from Bezacier et al. (2014). The densities of KCl-B1 and KCl-B2 (Dewaele et al., 2012) are shown as green and orange dotted dashed lines, respectively. The purple dashed line shows the density of antigorite from Bezacier et al. (2013).

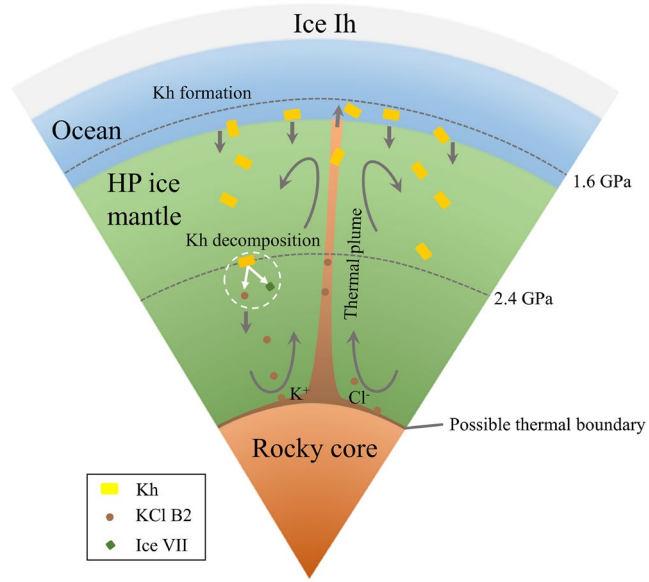

Figure 10. *Possible schematic internal structure and dynamics of an icy moon*. Thick gray arrows denote material upwelling and sinking. Thin gray arrows represent the idealized convective flow. The circles with white dashed lines represent the decomposition of the Kh into ice-VII and KCl-B2.

the density of KCl-bearing melts is lower than that of solid ices, the melts tend to upwell, and the Kh may crystallize again during the upwelling process. Thus, the formation and decomposition of Kh may play a role in inducing mantle convection in large icy moons and ocean exoplanets. We should note that this model is simplistic, as it only considers the densities and phase stabilities of KCl-H_2O compounds. Therefore, future studies should perform dynamic simulations that incorporate more information, such as viscosity, diffusion, and other solutes in the water system.

6. Conclusions

In this study, powder and SC-XRD, Raman and Brillouin scattering combined with DACs were used to investigate phase transformations, reactions and infer phase equilibria in the KCl-H_2O system for different KCl concentrations between 0 and 4 GPa and 298–405 K. We find that a novel KCl hydrate phase with $P2_1/n$ space group coexists with ice-VI and ice-VII at high pressures. During the revision of our manuscript, a study was also published reporting the synthesis of KCl monohydrate (Kh) with the same structure as our study (Yamashita et al., 2022). We propose a method to synthesize the single Kh crystal under high pressure straight from supersaturated KCl solutions. For the discovered Kh phase, we provide basic structural information that may help identify this phase in water-salts-bearing deep diamond inclusions. Based on our modeling, the formation and decomposition of Kh will contribute to the dynamic processes occurring inside icy moons and ocean exoplanets.

Data Availability Statement

All the experimental data and the data file for the crystal structure of KCl monohydrate phase can be found in the Wei (2022).

Acknowledgments
We acknowledge Monika Koch-Müller for her support on this project. We sincerely appreciate the valuable comments and suggestions provided by the two anonymous reviewers for this article. Xinyang Li, Qiang Zhou and Fangfei Li acknowledge supports from the National Natural Science Foundation of China (42102030, 12074141 and 12274168). Xinyang Li, Hanns-Peter Liermann, and Sergio Speziale acknowledge the scientific exchange and support of the Center for Molecular Water Science (CMWS) as part of the early science program (DESY and GFZ). This work was also supported by the Jilin Provincial Science and Technology Development Project (20210402054GH and 20210509038RQ) and the Program for Jilin University Science and Technology Innovative Research Team (No. 2021-TD-05). We also acknowledge DESY (Hamburg, Germany), a member of the Helmholtz Association HGF, for the provision of the experimental facilities. The X-ray diffraction was carried out at beamline P02.2 and used facilities provided by the Extreme Condition Science Infrastructure (ECSI) of PETRA III.

References

Abramson, E. H., & Brown, J. M. (2004). Equation of state of water based on speeds of sound measured in the diamond-anvil cell. *Geochimica et Cosmochimica Acta*, *68*(8), 1827–1835. https://doi.org/10.1016/j.gca.2003.10.020

Apelblat, A., & Manzurola, E. (1999). Volumetric properties of water, and solutions of sodium chloride and potassium chloride at temperatures from T = 277.15 K to T = 343.15 K at molalities of (0.1, 0.5, and 1.0) mol·kg^{-1}. *The Journal of Chemical Thermodynamics*, *31*(7), 869–893. https://doi.org/10.1006/jcht.1999.0487

Baumgartner, M., & Bakker, R. J. (2009). $CaCl_2$-hydrate nucleation in synthetic fluid inclusions. *Chemical Geology*, *265*(3), 335–344. https://doi.org/10.1016/j.chemgeo.2009.04.012

Bezacier, L., Journaux, B., Perrillat, J.-P., Cardon, H., Hanfland, M., & Daniel, I. (2014). Equations of state of ice VI and ice VII at high pressure and high temperature. *The Journal of Chemical Physics*, *141*(10), 104505. https://doi.org/10.1063/1.4894421

Bezacier, L., Reynard, B., Cardon, H., Montagnac, G., & Bass, J. D. (2013). High-pressure elasticity of serpentine and seismic properties of the hydrated mantle wedge. *Journal of Geophysical Research: Solid Earth*, *118*(2), 527–535. https://doi.org/10.1002/jgrb.50076

Bode, A. A. C., Pulles, P. G. M., Lutz, M., Poulisse, W. J. M., Jiang, S., Meijer, J. A. M., et al. (2015). Sodium chloride dihydrate crystals: Morphology, nucleation, growth, and inhibition. *Crystal Growth & Design*, *15*(7), 3166–3174. https://doi.org/10.1021/acs.cgd.5b00061

Bove, L. E., Gaal, R., Raza, Z., Ludl, A.-A., Klotz, S., Saitta Antonino, M., et al. (2015). Effect of salt on the H-bond symmetrization in ice. *Proceedings of the National Academy of Sciences of the United States of America*, *112*(27), 8216–8220. https://doi.org/10.1073/pnas.1502438112

Castillo-Rogez, J. C., & Lunine, J. I. (2010). Evolution of Titan's rocky core constrained by Cassini observations. *Geophysical Research Letters*, *37*(20), L20205. https://doi.org/10.1029/2010GL044398

Chivers, C. J., Buffo, J. J., & Schmidt, B. E. (2021). Thermal and chemical evolution of small, shallow water bodies in Europa's ice shell. *Journal of Geophysical Research: Planets*, *126*(5), e2020JE006692. https://doi.org/10.1029/2020JE006692

Chyba, C. F., & Hand, K. P. (2001). Life without photosynthesis. *Science*, *292*(5524), 2026–2027. https://doi.org/10.1126/science.1060081

Dewaele, A., Belonoshko, A. B., Garbarino, G., Occelli, F., Bouvier, P., Hanfland, M., & Mezouar, M. (2012). High-pressure--high-temperature equation of state of KCl and KBr. *Physical Review B*, *85*(21), 214105. https://doi.org/10.1103/PhysRevB.85.214105

Dolomanov, O. V., Bourhis, L. J., Gildea, R. J., Howard, J. A. K., & Puschmann, H. (2009). OLEX2: A complete structure solution, refinement and analysis program. *Journal of Applied Crystallography*, *42*(2), 339–341. https://doi.org/10.1107/S0021889808042726

Farrugia, L. (2012). WinGX and ORTEP for windows: An update. *Journal of Applied Crystallography*, *45*(4), 849–854. https://doi.org/10.1107/S0021889812029111

Fei, Y., Ricolleau, A., Frank, M., Mibe, K., Shen, G., & Prakapenka, V. (2007). Toward an internally consistent pressure scale. *Proceedings of the National Academy of Sciences of the United States of America*, *104*(22), 9182–9186. https://doi.org/10.1073/pnas.0609013104

Fortes, A. D. (2012). Titan's internal structure and the evolutionary consequences. *Planetary and Space Science*, *60*(1), 10–17. https://doi.org/10.1016/j.pss.2011.04.010

Fortes, A. D., & Choukroun, M. (2010). Phase behaviour of ices and hydrates. *Space Science Reviews*, *153*(1), 185–218. https://doi.org/10.1007/s11214-010-9633-3

Fortes, A. D., Grindrod, P. M., Trickett, S. K., & Vočadlo, L. (2007). Ammonium sulfate on Titan: Possible origin and role in cryovolcanism. *Icarus, International Journal of the Solar System*, *188*(1), 139–153. https://doi.org/10.1016/j.icarus.2006.11.002

Frank, M. R., Runge, C. E., Scott, H. P., Maglio, S. J., Olson, J., Prakapenka, V. B., & Shen, G. (2006). Experimental study of the NaCl–H_2O system up to 28 GPa: Implications for ice-rich planetary bodies. *Physics of the Earth and Planetary Interiors*, *155*(1), 152–162. https://doi.org/10.1016/j.pepi.2005.12.001

Frank, M. R., Scott, H. P., Aarestad, E., & Prakapenka, V. B. (2016). Potassium chloride-bearing ice VII and ice planet dynamics. *Geochimica et Cosmochimica Acta*, *174*, 156–166. https://doi.org/10.1016/j.gca.2015.11.027

Grimme, S., Antony, J., Ehrlich, S., & Krieg, H. (2010). A consistent and accurate ab initio parametrization of density functional dispersion correction (DFT-D) for the 94 elements H-Pu. *The Journal of Chemical Physics*, *132*(15), 154104. https://doi.org/10.1063/1.3382344

Hand, K. P., & Chyba, C. F. (2007). Empirical constraints on the salinity of the European ocean and implications for a thin ice shell. *Icarus, International Journal of the Solar System*, *189*(2), 424–438. https://doi.org/10.1016/j.icarus.2007.02.002

Hennings, E., Schmidt, H., & Voigt, W. (2013). Crystal structures of hydrates of simple inorganic salts. I. Water-rich magnesium halide hydrates $MgCl_2.8H_2O$, $MgCl_2.12H_2O$, $MgBr_2.6H_2O$, $MgBr_2.9H_2O$, $MgI_2.8H_2O$ and $MgI_2.9H_2O$. *Acta Crystallographica Section C*, *69*(11), 1292–1300. https://doi.org/10.1107/S0108270113028138

Hernandez, J.-A., Caracas, R., & Labrosse, S. (2022). Stability of high-temperature salty ice suggests electrolyte permeability in water-rich exoplanet icy mantles. *Nature Communications*, *13*(1), 3303. https://doi.org/10.1038/s41467-022-30796-5

Hönnerscheid, A., Nuss, J., Mühle, C., & Jansen, M. (2003). Die Kristallstrukturen der monohydrate von Lithiumchlorid und Lithiumbromid. *Zeitschrift für Anorganische und Allgemeine Chemie*, *629*(2), 312–316. https://doi.org/10.1002/zaac.200390049

Huang, Y., Nakatani, T., Nakamura, M., & McCammon, C. (2019). Saline aqueous fluid circulation in mantle wedge inferred from olivine wetting properties. *Nature Communications*, *10*(1), 5557. https://doi.org/10.1038/s41467-019-13513-7

Jones, G., Taylor, E. F., & Vogel, R. C. (1948). The apparent molal expansibilities of potassium, barium and lanthanum chlorides as a function of concentration and Temperature[1]. *Journal of the American Chemical Society*, *70*(3), 966–977. https://doi.org/10.1021/ja01183a023

Journaux, B. (2022). Salty ice and the dilemma of ocean exoplanet habitability. *Nature Communications*, *13*(1), 3304. https://doi.org/10.1038/s41467-022-30799-2

Journaux, B., Daniel, I., Caracas, R., Montagnac, G., & Cardon, H. (2013). Influence of NaCl on ice VI and ice VII melting curves up to 6 GPa, implications for large icy moons. *Icarus, International Journal of the Solar System*, *226*(1), 355–363. https://doi.org/10.1016/j.icarus.2013.05.039

Journaux, B., Daniel, I., Petitgirard, S., Cardon, H., Perrillat, J.-P., Caracas, R., & Mezouar, M. (2017). Salt partitioning between water and high-pressure ices. Implication for the dynamics and habitability of icy moons and water-rich planetary bodies. *Earth and Planetary Science Letters*, *463*, 36–47. https://doi.org/10.1016/j.epsl.2017.01.017

Journaux, B., Kalousová, K., Sotin, C., Tobie, G., Vance, S., Saur, J., et al. (2020). Large ocean worlds with high-pressure ices. *Space Science Reviews*, *216*(1), 7. https://doi.org/10.1007/s11214-019-0633-7

Journaux, B., Pakhomova, A., Collings, I. E., Petitgirard, S., Boffa Ballaran, T., Brown, J. M., et al. (2023). On the identification of hyperhydrated sodium chloride hydrates, stable at icy moon conditions. *Proceedings of the National Academy of Sciences of the United States of America*, *120*(9), e2217125120. https://doi.org/10.1073/pnas.2217125120

Kell, G. S., & Whalley, E. (1975). Reanalysis of the density of liquid water in the range 0–150°C and 0–1 kbar. *The Journal of Chemical Physics*, *62*(9), 3496–3503. https://doi.org/10.1063/1.430986

Khurana, K. K., Kivelson, M. G., Stevenson, D. J., Schubert, G., Russell, C. T., Walker, R. J., & Polanskey, C. (1998). Induced magnetic fields as evidence for subsurface oceans in Europa and Callisto. *Nature*, *395*(6704), 777–780. https://doi.org/10.1038/27394

Kivelson, M. G., Khurana, K. K., Russell, C. T., Volwerk, M., Walker, R. J., & Zimmer, C. (2000). Galileo magnetometer measurements: A stronger case for a subsurface ocean at Europa. *Science*, *289*(5483), 1340–1343. https://doi.org/10.1126/science.289.5483.1340

Klewe, B., & Pedersen, B. (1974). The crystal structure of sodium chloride dihydrate. *Acta Crystallographica Section B*, *30*(10), 2363–2371. https://doi.org/10.1107/S0567740874007138

Klotz, S., Bove, L. E., Strässle, T., Hansen, T. C., & Saitta, A. M. (2009). The preparation and structure of salty ice VII under pressure. *Nature Materials*, *8*(5), 405–409. https://doi.org/10.1038/nmat2422

Klotz, S., Komatsu, K., Pietrucci, F., Kagi, H., Ludl, A. A., Machida, S., et al. (2016). Ice VII from aqueous salt solutions: From a glass to a crystal with broken H-bonds. *Scientific Reports*, *6*(1), 32040. https://doi.org/10.1038/srep32040

Komatsu, K., Shinozaki, A., Machida, S., Matsubayashi, T., Watanabe, M., Kagi, H., et al. (2015). Crystal structure of magnesium dichloride decahydrate determined by X-ray and neutron diffraction under high pressure. *Acta Crystallographica Section B*, *71*(1), 74–80. https://doi.org/10.1107/S205252061500027X

Kresse, G., & Furthmüller, J. (1996a). Efficiency of ab-initio total energy calculations for metals and semiconductors using a plane-wave basis set. *Computational Materials Science*, *6*(1), 15–50. https://doi.org/10.1016/0927-0256(96)00008-0

Kresse, G., & Furthmüller, J. (1996b). Efficient iterative schemes for ab initio total-energy calculations using a plane-wave basis set. *Physical Review B*, *54*(16), 11169–11186. https://doi.org/10.1103/PhysRevB.54.11169

Kresse, G., & Joubert, D. (1999). From ultrasoft pseudopotentials to the projector augmented-wave method. *Physical Review B*, *59*(3), 1758–1775. https://doi.org/10.1103/PhysRevB.59.1758

Lammer, H., Bredehöft, J. H., Coustenis, A., Khodachenko, M. L., Kaltenegger, L., Grasset, O., et al. (2009). What makes a planet habitable? *Astronomy and Astrophysics Review*, *17*(2), 181–249. https://doi.org/10.1007/s00159-009-0019-z

Lauro, S. E., Pettinelli, E., Caprarelli, G., Guallini, L., Rossi, A. P., Mattei, E., et al. (2021). Multiple subglacial water bodies below the south pole of Mars unveiled by new MARSIS data. *Nature Astronomy*, *5*(1), 63–70. https://doi.org/10.1038/s41550-020-1200-6

Li, F., Cui, Q., He, Z., Cui, T., Zhang, J., Zhou, Q., et al. (2005). High pressure-temperature Brillouin study of liquid water: Evidence of the structural transition from low-density water to high-density water. *The Journal of Chemical Physics*, *123*(17), 174511. https://doi.org/10.1063/1.2102888

Liermann, H.-P., Konopkova, Z., Morgenroth, W., Glazyrin, K., Bednarcik, J., McBride, E. E., et al. (2015). The Extreme conditions beamline P02.2 and the Extreme conditions science infrastructure at PETRA III. *Journal of Synchrotron Radiation*, *22*(4), 908–924. https://doi.org/10.1107/S1600577515005937

Logvinova, A., Zedgenizov, D., & Wirth, R. (2019). Specific multiphase assemblages of carbonatitic and Al-rich silicic diamond-forming fluids/melts: TEM observation of microinclusions in cuboid diamonds from the placers of northeastern Siberian craton. *Minerals*, *9*(1), 50. https://doi.org/10.3390/min9010050

Ludl, A. A., Bove, L. E., Corradini, D., Saitta, A. M., Salanne, M., Bull, C. L., & Klotz, S. (2017). Probing ice VII crystallization from amorphous NaCl–D_2O solutions at gigapascal pressures. *Physical Chemistry Chemical Physics*, *19*(3), 1875–1883. https://doi.org/10.1039/C6CP07340A

Mantegazzi, D., Sanchez-Valle, C., & Driesner, T. (2013). Thermodynamic properties of aqueous NaCl solutions to 1073 K and 4.5 GPa, and implications for dehydration reactions in subducting slabs. *Geochimica et Cosmochimica Acta*, *121*, 263–290. https://doi.org/10.1016/j.gca.2013.07.015

Momma, K., & Izumi, F. (2011). VESTA 3 for three-dimensional visualization of crystal, volumetric and morphology data. *Journal of Applied Crystallography*, *44*(6), 1272–1276. https://doi.org/10.1107/S0021889811038970

Nakamura, R., & Ohtani, E. (2011). The high-pressure phase relation of the $MgSO_4$–H_2O system and its implication for the internal structure of Ganymede. *Icarus, International Journal of the Solar System*, *211*(1), 648–654. https://doi.org/10.1016/j.icarus.2010.08.029

Niemann, H. B., Atreya, S. K., Bauer, S. J., Carignan, G. R., Demick, J. E., Frost, R. L., et al. (2005). The abundances of constituents of Titan's atmosphere from the GCMS instrument on the Huygens probe. *Nature*, *438*(7069), 779–784. https://doi.org/10.1038/nature04122

Nimmo, F., & Pappalardo, R. T. (2016). Ocean worlds in the outer solar system. *Journal of Geophysical Research: Planets*, *121*(8), 1378–1399. https://doi.org/10.1002/2016JE005081

Noack, L., Höning, D., Rivoldini, A., Heistracher, C., Zimov, N., Journaux, B., et al. (2016). Water-rich planets: How habitable is a water layer deeper than on Earth? *Icarus, International Journal of the Solar System*, *277*, 215–236. https://doi.org/10.1016/j.icarus.2016.05.009

Pabalan, R. T., & Pitzer, K. S. (1988). Apparent molar heat capacity and other thermodynamic properties of aqueous potassium chloride solutions to high temperatures and pressures. *Journal of Chemical and Engineering Data*, *33*(3), 354–362. https://doi.org/10.1021/je00053a037

Perdew, J. P., Burke, K., & Wang, Y. (1996). Generalized gradient approximation for the exchange-correlation hole of a many-electron system. *Physical Review B*, *54*(23), 16533–16539. https://doi.org/10.1103/PhysRevB.54.16533

Perdew, J. P., & Wang, Y. (1992). Accurate and simple analytic representation of the electron-gas correlation energy. *Physical Review B*, *45*(23), 13244–13249. https://doi.org/10.1103/PhysRevB.45.13244

Pistorius, C. W. F. T., Rapoport, E., & Clark, J. B. (1968). Phase diagrams of H_2O and D_2O at high pressures. *The Journal of Chemical Physics*, *48*(12), 5509–5514. https://doi.org/10.1063/1.1668248

Postberg, F., Kempf, S., Schmidt, J., Brilliantov, N., Beinsen, A., Abel, B., et al. (2009). Sodium salts in E-ring ice grains from an ocean below the surface of Enceladus. *Nature*, *459*(7250), 1098–1101. https://doi.org/10.1038/nature08046

Prescher, C., & Prakapenka, V. B. (2015). DIOPTAS: A program for reduction of two-dimensional X-ray diffraction data and data exploration. *High Pressure Research*, *35*(3), 223–230. https://doi.org/10.1080/08957959.2015.1059835

Romanenko, A. V., Rashchenko, S. V., Kurnosov, A., Dubrovinsky, L., Goryainov, S. V., Likhacheva, A. Y., & Litasov, K. D. (2018). Single-standard method for simultaneous pressure and temperature estimation using Sm^{2+}: SrB_4O_7 fluorescence. *Journal of Applied Physics*, *124*(16), 165902. https://doi.org/10.1063/1.5046144

Romankiw, L. A., & Chou, I. M. (1983). Densities of aqueous sodium chloride, potassium chloride, magnesium chloride, and calcium chloride binary solutions in the concentration range 0.5-6.1 m at 25, 30, 35, 40, and 45°C. *Journal of Chemical and Engineering Data*, *28*(3), 300–305. https://doi.org/10.1021/je00033a005

Sandercock, J. R. (1980). Light scattering from thermally excited surface phonons and magnons. In W. F. Murphy (Ed.), *Paper presented at the Proceedings of the 7th international conference on Raman spectroscopy*. North-Holland.

Schmidt, C., & Manning, C. E. (2016). Pressure-induced ion pairing in $MgSO_4$ solutions: Implications for the oceans of icy worlds. *Geochemical Perspectives Letters*, *3*, 66–74. https://doi.org/10.7185/geochemlet.1707

Schubert, G., Hussmann, H., Lainey, V., Matson, D. L., McKinnon, W. B., Sohl, F., et al. (2010). Evolution of icy satellites. *Space Science Reviews*, *153*(1), 447–484. https://doi.org/10.1007/s11214-010-9635-1

Sheldrick, G. (2015). Crystal structure refinement with SHELXL. *Acta Crystallographica Section C*, *71*(1), 3–8. https://doi.org/10.1107/S2053229614024218

Shen, G., Wang, Y., Dewaele, A., Wu, C., Fratanduono, D. E., Eggert, J., et al. (2020). Toward an international practical pressure scale: A proposal for an IPPS ruby gauge (IPPS-Ruby2020). *High Pressure Research*, *40*(3), 299–314. https://doi.org/10.1080/08957959.2020.1791107

Smith, E. M., Kopylova, M. G., Dubrovinsky, L., Navon, O., Ryder, J., & Tomlinson, E. L. (2011). Transmission X-ray diffraction as a new tool for diamond fluid inclusion studies. *Mineralogical Magazine*, *75*(5), 2657–2675. https://doi.org/10.1180/minmag.2011.075.5.2657

Sugimoto, K., Dinnebier, R. E., & Hanson, J. C. (2007). Structures of three dehydration products of bischofite from in situ synchrotron powder diffraction data ($MgCl_2.nH_2O$; n = 1, 2, 4). *Acta Crystallographica Section B*, *63*(2), 235–242. https://doi.org/10.1107/S0108768107002558

Tschauner, O., Huang, S., Greenberg, E., Prakapenka, V. B., Ma, C., Rossman, G. R., et al. (2018). Ice-VII inclusions in diamonds: Evidence for aqueous fluid in Earth's deep mantle. *Science*, *359*(6380), 1136–1139. https://doi.org/10.1126/science.aao3030

Tsironi, I., Schlesinger, D., Späh, A., Eriksson, L., Segad, M., & Perakis, F. (2020). Brine rejection and hydrate formation upon freezing of NaCl aqueous solutions. *Physical Chemistry Chemical Physics*, *22*(14), 7625–7632. https://doi.org/10.1039/C9CP05436G

Uriarte, L. M., Dubessy, J., Boulet, P., Baonza, V. G., Bihannic, I., & Robert, P. (2015). Reference Raman spectra of synthesized $CaCl_2{\cdot}nH_2O$ solids (n = 0, 2, 4, 6). *Journal of Raman Spectroscopy*, *46*(10), 822–828. https://doi.org/10.1002/jrs.4730

Valenti, P., Bodnar, R. J., & Schmidt, C. (2012). Experimental determination of H_2O–NaCl liquidi to 25 mass% NaCl and 1.4 GPa: Application to the Jovian satellite Europa. *Geochimica et Cosmochimica Acta*, *92*, 117–128. https://doi.org/10.1016/j.gca.2012.06.007

Vance, S., Bouffard, M., Choukroun, M., & Sotin, C. (2014). Ganymede's internal structure including thermodynamics of magnesium sulfate oceans in contact with ice. *Planetary and Space Science*, *96*, 62–70. https://doi.org/10.1016/j.pss.2014.03.011

Vance, S., Journaux, B., Hesse, M., & Steinbrügge, G. (2021). The salty secrets of icy ocean worlds. *Journal of Geophysical Research: Planets*, *126*(1), e2020JE006736. https://doi.org/10.1029/2020JE006736

Walker, D., Cranswick, L. M. D., Verma, P. K., Clark, S. M., & Buhre, S. (2002). Thermal equations of state for B1 and B2 KCl. *American Mineralogist*, *87*(7), 805–812. https://doi.org/10.2138/am-2002-0701

Wei, X. (2022). Novel high-pressure potassium chloride monohydrate and its implications for water-rich planetary bodies [Dataset]. Zenodo. https://doi.org/10.5281/zenodo.7972917

Whitfield, C. H., Brody, E. M., & Bassett, W. A. (1976). Elastic moduli of NaCl by Brillouin scattering at high pressure in a diamond anvil cell. *Review of Scientific Instruments*, *47*(8), 942–947. https://doi.org/10.1063/1.1134778

Wiryana, S., Slutsky, L. J., & Brown, J. M. (1998). The equation of state of water to 200°C and 3.5 GPa: Model potentials and the experimental pressure scale. *Earth and Planetary Science Letters*, *163*(1), 123–130. https://doi.org/10.1016/S0012-821X(98)00180-0

Yamashita, K., Komatsu, K., & Kagi, H. (2022). Crystal structure of potassium chloride monohydrate: Water intercalation into the B1 structure of KCl under high pressure. *Acta Crystallographica Section C*, *78*(12), 749–754. https://doi.org/10.1107/S2053229622011135

Yoshimura, Y., Mao, H.-K., & Hemley, R. J. (2004). Transformation of ice in aqueous KCl solution to a high-pressure, low-temperature phase. *Chemical Physics Letters*, *400*(4), 511–514. https://doi.org/10.1016/j.cplett.2004.10.139

Zimmer, C., Khurana, K. K., & Kivelson, M. G. (2000). Subsurface Oceans on Europa and Callisto: Constraints from Galileo magnetometer observations. *Icarus*, *147*(2), 329–347. https://doi.org/10.1006/icar.2000.6456

Zolensky, M. E. (2005). Extraterrestrial water. *Elements*, *1*(1), 39–43. https://doi.org/10.2113/gselements.1.1.39

Zolotov, M. Y. (2012). Aqueous fluid composition in CI chondritic materials: Chemical equilibrium assessments in closed systems. *Icarus, International Journal of the Solar System*, *220*(2), 713–729. https://doi.org/10.1016/j.icarus.2012.05.036

Zolotov, M. Y., & Shock, E. L. (2001). Composition and stability of salts on the surface of Europa and their oceanic origin. *Journal of Geophysical Research*, *106*(E12), 32815–32827. https://doi.org/10.1029/2000JE001413